THE ASTROPHYSICAL JOURNAL, 499:414–428, 1998 May 20

HUBBLE SPACE TELESCOPE ECLIPSE OBSERVATIONS OF THE NOVA-LIKE CATACLYSMIC VARIABLE UX URSAE MAJORIS[1]

CHRISTIAN KNIGGE AND KNOX S. LONG
Space Telescope Science Institute, 3700 San Martin Drive, Baltimore, MD 21218; knigge@stsci.edu, long@stsci.edu
RICHARD A. WADE
Pennsylvania State University, Department of Astronomy and Astrophysics, 525 Davey Laboratory, University Park, PA 16802; wade@astro.psu.edu
RAYMUNDO BAPTISTA
Departamento de Física, Universidade Federal de Santa Catarina, Campus Universitario, Trindade, 88040 Florianopolis, Brazil; bap@fsc.ufsc.br
KEITH HORNE
Department of Physics and Astronomy, University of St. Andrews, North Haugh, St. Andrews, Fife, KY16 9SS, Scotland, UK; kdh1@st-andrews.ac.uk
IVAN HUBENY
NASA Goddard Space Flight Center, Greenbelt, MD 20771; hubeny@stars.gsfc.nasa.gov
AND
RENÉ G. M. RUTTEN
Isaac Newton Group, Apartado de Correos 321, E-38730 Santa Cruz de la Palma, Spain; rgmr@ing.iac.es
Received 1997 August 6; accepted 1997 December 19

ABSTRACT

We present and analyze *Hubble Space Telescope* observations of the eclipsing nova-like cataclysmic variable UX UMa obtained with the *Faint Object Spectrograph*. Two eclipses each were observed with the G160L grating (covering the ultraviolet waveband) in 1994 August and with the PRISM (covering the near-ultraviolet to near-infrared) in November of the same year. The system was $\sim 50\%$ brighter in November than in August, which, if due to a change in the accretion rate, indicates a fairly substantial increase in $\dot{M}_{\rm acc}$ by $\gtrsim 50\%$. The eclipse light curves are qualitatively consistent with the gradual occultation of an accretion disk with a radially decreasing temperature distribution. The light curves also exhibit asymmetries about mideclipse that are likely due to a bright spot at the disk edge. Bright-spot spectra have been constructed by differencing the mean spectra observed at pre- and posteclipse orbital phases. These difference spectra contain ultraviolet absorption lines and show the Balmer jump in emission. This suggests that part of the bright spot may be optically thin in the continuum and vertically extended enough to veil the inner disk and/or the outflow from UX UMa in some spectral lines. Model disk spectra constructed as ensembles of stellar atmospheres provide poor descriptions of the observed posteclipse spectra, despite the fact that UX UMa's light should be dominated by the disk at this time. Suitably scaled single temperature model stellar atmospheres with $T_{\rm eff} \simeq 12{,}500$–$14{,}500$ K actually provide a better match to both the ultraviolet and optical posteclipse spectra. Evidently, great care must be taken in attempts to derive accretion rates from comparisons of disk models to observations. One way to reconcile disk models with the observed posteclipse spectra is to postulate the presence of a significant amount of optically thin material in the system. Such an optically thin component might be associated with the transition region ("chromosphere") between the disk photosphere and the fast wind from the system, whose presence has been suggested by Knigge & Drew. In any event, the wind/chromosphere is likely to be the region in which many, if not most, of the UV lines are formed. This is clear from the plethora of emission lines that appear in the mideclipse spectra, some of which appear as absorption features in spectra taken at out-of-eclipse orbital phases.

Subject headings: accretion, accretion disks — binaries: close — novae, cataclysmic variables — stars: individual (UX Ursae Majoris) — ultraviolet: stars

1. INTRODUCTION

Nova-like (NL) cataclysmic variables (CVs) provide a unique opportunity to study the process of disk accretion in what is likely to be its simplest form. These systems are semidetached binary stars, in which mass is transferred from a Roche lobe filling, low-mass, late-type secondary onto an accretion disk around a mass-gaining dwarf (WD) primary. NLs have relatively constant light curves, unlike another class of disk-accreting CVs, the dwarf-novae (DNs), which undergo 3–5 mag outbursts on timescales of weeks to months. The difference between NLs and DNs is probably related to the rate at which mass is transferred from the secondary onto the disk (Meyer & Meyer-Hofmeister 1983; Smak 1983). In DNs this accretion rate is below some critical value, and the disk oscillates between a low-viscosity, optically thin, quiescent state and a high-viscosity, optically thick, outburst state. In NL variables, on the other hand, the accretion rate is higher, and the disk is always in the optically thick high state. Since accretion disk theory should be on firmest ground when steady state, optically thick conditions may reasonably be assumed, observations of NLs provide an excellent test bed for our basic understanding of accretion disk physics.

[1] Based on observations with the NASA/ESA *Hubble Space Telescope*, obtained at the Space Telescope Science Institute, which is operated by the Association of Universities for Research in Astronomy, Inc., under NASA contract NAS 5-2655.

Observations of eclipsing systems are particularly important in this respect because phase-resolved light curves around orbital phase $\phi_{\rm orb} = 0.0$ (when the secondary star is in front of the disk and WD as seen from Earth) contain information about the spatial brightness distribution of the accretion disk and other system components (e.g., Horne 1985). Here, we present eclipse observations of the NL variable UX UMa obtained with the Faint Object Spectrograph (FOS) on the *Hubble Space Telescope* (*HST*). The data cover four primary eclipses with high time resolution and extend over a total wavelength range of nearly 7000 Å. The purpose of the present paper is to describe the observations and to determine the spectral properties of the system components that can be isolated in the time-resolved spectra (the accretion disk, the uneclipsed light, and the bright spot). We have also detected coherent 29 s dwarf nova-type oscillations in some of the data, which will be analyzed in a companion paper (Knigge et al. 1998a, hereafter Paper II; see Warner & Nather 1972 and Nather & Robinson 1974 for previous detections of UX UMa's 29 s oscillations). Eclipse mapping studies based on this data set, using both direct model fitting and image reconstruction techniques, are also being carried out and will be presented separately (Knigge et al. 1998b, hereafter Paper III; Baptista et al. 1998, hereafter Paper IV).

2. OBSERVATIONS

The target of our observations, UX UMa, is a bright ($V \simeq 12.8$), eclipsing nova-like variable with an orbital period of 4.72 hr (Kukarkin 1977). Its system parameters have recently been derived by Baptista et al. (1995), and we will not attempt to refine them here. Instead, we list Baptista et al.'s values in Table 1 for reference and will assume them throughout the paper unless explicitly noted otherwise.

UX UMa was observed with the FOS on board the *HST* in 1994 August and November. For the August observations, the G160L grating on the BLUE digicon (nominal wavelength coverage 1140–2508 Å) was used with the 1.0 (0.″6 diameter) aperture; in November, the PRISM on the RED digicon (nominal wavelength coverage 1850–1950 Å) was used with the 4.3 (3.″66 × 3.″71) aperture. This combination of gratings gives the widest overall wavelength coverage that was obtainable with the FOS, at the price of relatively low spectral resolution. The spectral resolution of the G160L was 6.6 Å FWHM with our instrumental setup, and that of the PRISM, which has a highly non-uniform dispersion, varied from about 4 Å near the short-wavelength end to more than 400 Å at the longest wavelengths. Two eclipses were observed in both epochs. The two August sequences covered consecutive orbital cycles, but the November sequences were separated by two unobserved eclipses. All observations were carried out in RAPID mode, with a new exposure beginning approximately every 5.4 s. A log of the four observing sequences is given in Table 2.

TABLE 1

ADOPTED SYSTEM PARAMETERS[a]

Parameter	Value
$q = M_2/M_1$	1.0 ± 0.1
i	71.0 ± 0.6
$M_1/M_\odot$	0.47 ± 0.07
$M_2/M_\odot$	0.47 ± 0.1
$R_1/R_\odot$	0.014 ± 0.001
$R_2/R_\odot$[b]	0.53 ± 0.04
$a/R_\odot$	1.39 ± 0.08

[a] From Baptista et al. 1995.

[b] The value listed for R_2, the volume-averaged radius of the secondary star, is 4% larger than that give by Baptista et al. 1995. The new value was derived using a more accurate formula for R_2/a.

All of the observations occurred normally, with the target well centered in the aperture. The data were reduced using the standard STSDAS pipeline software with the set of calibration files that was available in 1996 May. STSDAS pipeline reduction includes flat-fielding corrections, background subtraction, as well as wavelength and absolute flux calibrations. To avoid having to apply additional and uncertain corrections for geocoronal, dark-current, and second-order contributions, we have restricted our analysis of the data to somewhat smaller than nominal wavelength regions, namely, 1230–2300 Å for the G160L spectra and 2000–8000 Å for the PRISM spectra. The photometric accuracy of the reduced spectra should be about 4%.

In observations with the G160L grating, the zeroth-order undispersed light is also recorded and can be used to construct a broadband optical-UV light curve. The zeroth-order light has a bandpass with full width at half-response of 1900 Å and a pivot wavelength of 3400 Å. The G160L zeroth-order photometry has so far only been flux-calibrated against pre-COSTAR observations (Horne & Eracleous 1993; Eracleous & Horne 1994), but Eracleous & Horne (1994) do predict a post-COSTAR response of 950 counts s^{-1} mJy^{-1} [$\simeq 3.7 \times 10^{17}$ counts s^{-1} (ergs s^{-1} $Å^{-1})^{-1}$] for our instrumental setup. This calibration is, however, not very precise, as even the pre-COSTAR response is only accurate to about 50% (Eracleous & Horne 1994).

Continuum light curves were constructed from the first-order data for a number of wavelength bands as shown in Figures 1 and 2. These bands cover the observed spectral range but avoid obviously line-blanketed regions and strong emission/absorption features. The phase-averaged mid-eclipse spectra (see below) proved to be particularly useful

TABLE 2

JOURNAL OF OBSERVATIONS

Run	Date (1994)	UT Start	UT End	Phase Range (Cycles)	Number of Spectra	Grating	Detector	Aperture	Wavelength Range (Å)
1.....	Aug 03	02:53	03:55	0.91–1.13	691	G160L	BLUE	1.0	1140–2508
2.....	Aug 03	07:43	08:45	0.94–1.16	691	G160L	BLUE	1.0	1140–2508
3.....	Nov 11	04:34	05:52	0.84–1.11	870	PRISM	RED	4.3	1850–8950
4.....	Nov 11	18:55	20:13	0.88–1.16	870	PRISM	RED	4.3	1850–8950

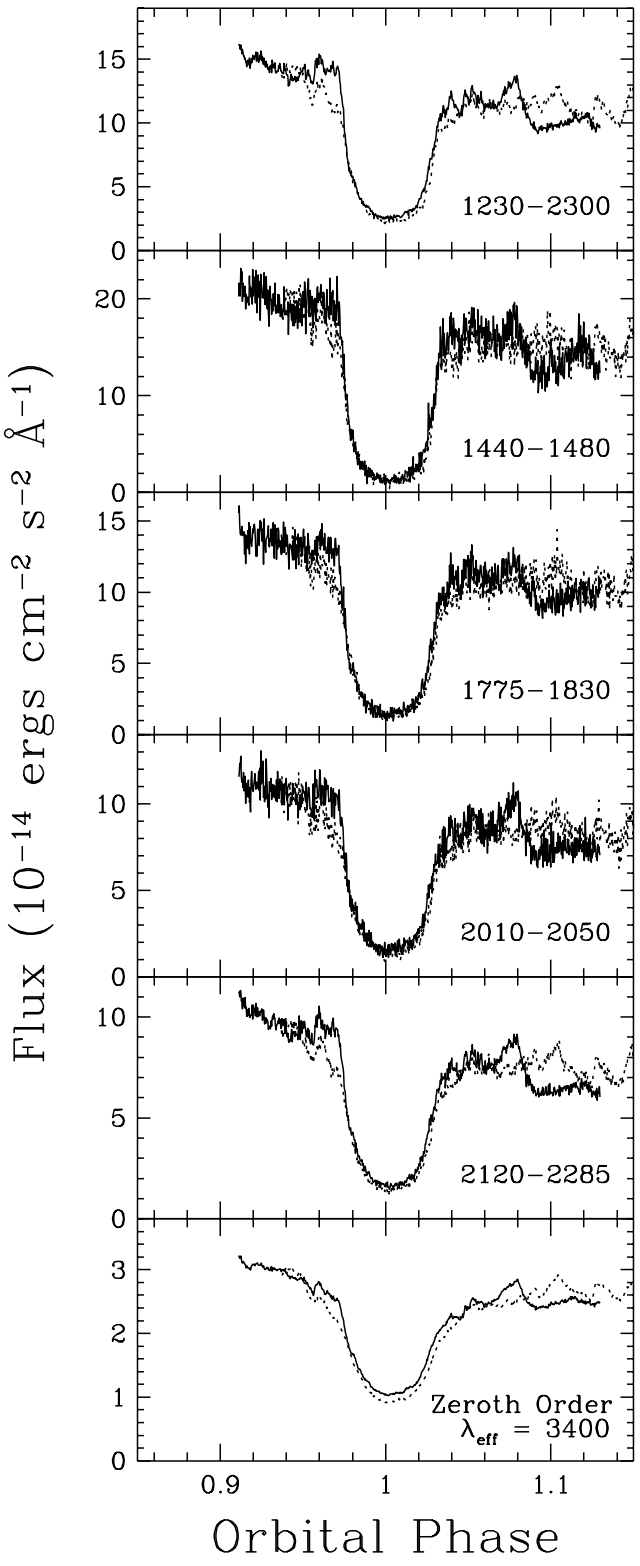

FIG. 1.—Continuum light curves constructed from the August (G160L) observing sequences (run 1, *solid lines*; run 2, *dotted lines*) phased according to the ephemeris of Baptista et al. (1995). The wavelength ranges over which the spectra were averaged to obtain the light curves are given (in angstroms) at the bottom right of each panel; for the zeroth-order light curves the effective wavelength of the bandpass is given.

in selecting suitable continuum windows. Each light curve was computed by averaging the flux within a given continuum band for each spectrum in a given observing sequence and phasing the data according to the linear ephemeris given by Baptista et al. (1995). In addition to these continuum light curves, Figures 1 and 2 also show high S/N, "white-light" light curves that have been constructed as time series of the average fluxes over the full adopted wavelength range of each grating. For the two G160L observing sequences, the zeroth-order light curves, calibrated according to the response estimate given above, are also plotted in Figure 1.

The spectral properties of the various system components in UX UMa are most easily investigated by relying on mean spectra obtained by averaging over suitable orbital phase ranges. For the present study, mean pre-, mid- and post-eclipse spectra are required, which have been calculated as averages over the following phase ranges:

1. Preeclipse: $\phi < 0.95$.
2. Mideclipse: $0.98 < \phi < 1.02$.
3. Posteclipse: $\phi > 1.04$.

These spectra are shown in Figures 3 and 4, which also give suggested identifications for the strongest emission and absorption lines in the spectra.

Since the shape and apparent magnitude of UX UMa's spectrum could be affected by interstellar reddening, we have inspected all mean spectra for evidence of the characterisic 2175 Å dust absorption feature. None was found, consistent with the nondetection of the same reddening indicator in an analysis of *IUE* spectra (Verbunt 1987). Consequently, we adopt $E(B-V) = 0.0$ as our preferred estimate but will consider values as high as Verbunt's upper limit of $E(B-V) = 0.04$ where our conclusions might otherwise depend on this.

3. ANALYSIS OF LIGHT CURVES

3.1. *General Characteristics*

Overall, the light curves in Figures 1 and 2 are typical of eclipsing NL variables and DNs in outburst (e.g., Rutten, van Paradijs, & Tinbergen 1992). Specifically, from short to long wavelengths, the eclipses become increasingly broad and shallow, and the out-of-eclipse flux level drops off. This is consistent with the eclipse of an accretion disk with a relatively blue spectrum (see § 4.2) and a temperature distribution that decreases with radius. Substantial short-timescale variations unrelated to the eclipse, "flickering," are also seen. This, too, is common among NLs and DNs.

All of the light curves are asymmetric. At wavelengths below the Balmer jump at 3646 Å, the asymmetry manifests itself primarily as a difference between the pre- and post-eclipse flux levels. Thus, even though the deep eclipse of the central parts of the disk appears to be over at orbital phases $\phi \gtrsim 1.04$, the fluxes have recovered to just 50%–80% of the preeclipse level at this point. Beyond this, the posteclipse flux at these wavelengths remains roughly constant to the end of the observing sequences. At longer wavelengths, the asymmetry is perhaps better described as an extended eclipse egress relative to ingress. However, even at these wavelengths the preeclipse flux level is never fully recovered.

Asymmetries of this type could result from orbital phase-dependent absorption in the system. More conventionally, they tend to be attributed to a "bright spot" (BS) produced by the impact of the accretion stream from the secondary onto the disk edge. Since the stream leads the secondary, the BS should be located in the quadrant of the disk between phases 0.75 and 1.0. If (part of) the BS can be described as a

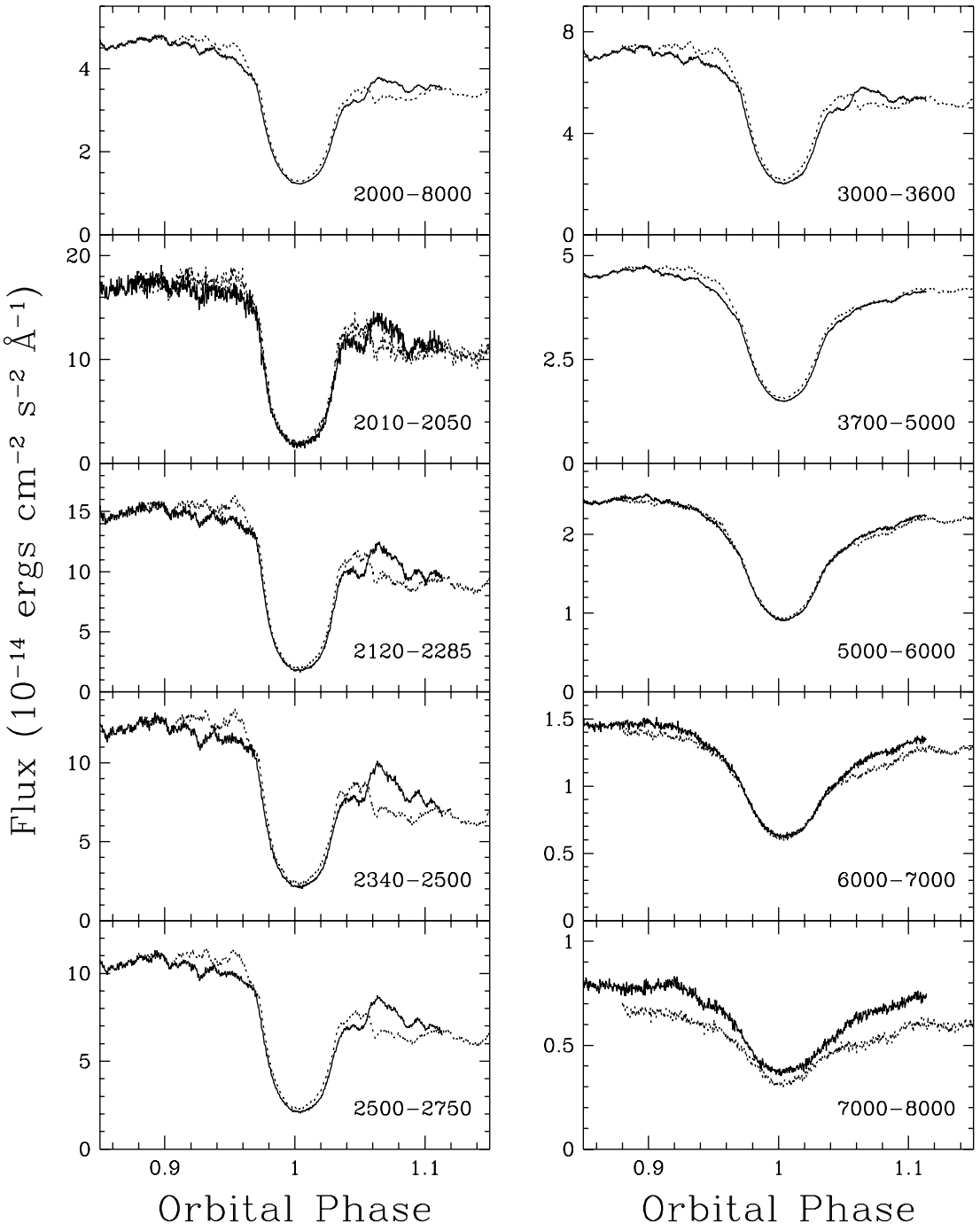

FIG. 2.—Continuum light curves constructed from the November (PRISM) observing sequences (run 3, *solid lines*; run 4, *dotted lines*) phased according to the ephemeris of Baptista et al. (1995). The wavelength ranges over which the spectra were averaged to obtain the light curves are given (in angstroms) at the bottom right of each panel.

spot painted on the outside of the disk rim, it will be visible for about half an orbital cycle. During this time, its uneclipsed light curve should be roughly sinusoidal, with the maximum occurring when the spot is facing the observer. The BS can also be eclipsed by the secondary, but due to its position at the disk edge and off the line of centers of the two stars, mid-eclipse for the BS will be delayed with respect to the time of conjunction.

Most of the characteristic features of the light curves in Figures 1 and 2 can be interpreted within this framework. The failure of all light curves to recover their preeclipse flux levels after conjunction implies that the BS eclipse lasts until close to the end of the observing runs and/or that the BS light is near maximum at preeclipse phases, so that its contribution at posteclipse phases is diminished. The difference between the light-curve morphologies at short and long wavelengths can also be understood qualitatively. If the BS is relatively compact, the width of its eclipses will be the same at all wavelengths. Disk eclipses, on the other hand, will widen at longer wavelengths, where the cool outer parts of the disk contribute relatively more to the flux. A superposition of spot and disk light curves might therefore be able to reproduce the observed light-curve shapes. We will test this interpretation quantitatively in Paper III.

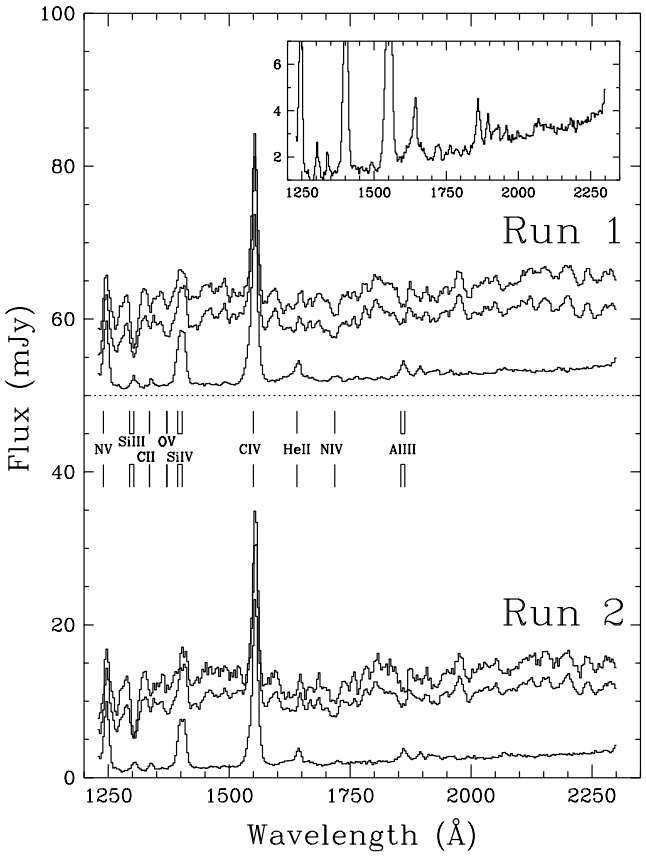

FIG. 3.—Average pre-, mid-, and posteclipse spectra for runs 1 and 2. The dotted horizontal line marks the zero level for the run 1 spectra. The inset shows the run 1 mideclipse spectrum on a scale more appropriate for inspection of the weaker emission lines in this spectrum. For both runs, the highest (middle, lowest) spectrum corresponds to the average over pre- (post-, mid-) eclipse orbital phases.

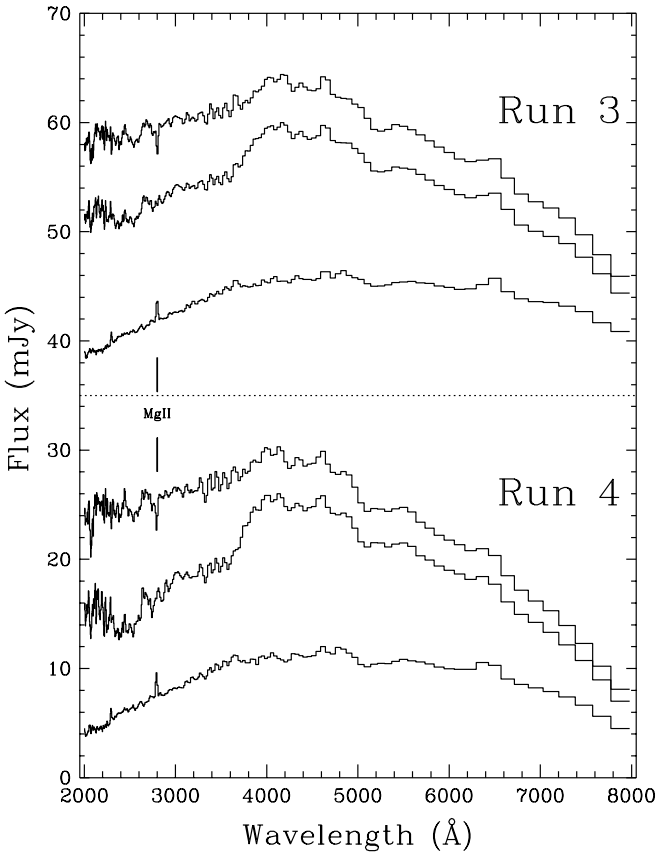

FIG. 4.—Average pre, mid-, and posteclipse spectra for runs 3 and 4. The dotted horizontal line marks the zero level for the run 3 spectra. For both runs, the highest (middle, lowest) spectrum corresponds to the average over pre- (post-, mid-) eclipse orbital phases.

Apart from short-timescale variations away from eclipse, the light curves constructed from runs 1 and 2 (G160L) are similar, as are the run 3 and run 4 (PRISM) light curves. The main exceptions are the longest wavelength (7000–8000 Å) PRISM light curves, which show an $\sim 20\%$ flux decrease between runs 3 and 4. Since only the red end of the spectrum is affected, this brightness change may be related to a change in the cool, outer parts of the disk.

The continuum light curves between 2000 and 2300 Å, which are common to the G160L and PRISM observing sequences, show that UX UMa was about 50% brighter in November than in August. If interpreted as reflecting a change in the accretion rate, a 50% flux increase in this wavelength region corresponds to an increase in $\dot{M}_{\rm acc}$ by $\gtrsim 50\%$ in the optically thick disk model spectra described in § 4, for all accretion rates $\gtrsim 10^{17}$ g s^{-1}. From the overlap region of the pre- and posteclipse spectra described in § 4, we find that the ratios of the pre- and posteclipse levels in November ($\simeq 1.2$–1.4) were similar, although slightly larger than those in the August data ($\simeq 1.4$–1.7). Thus the BS and the disk appear to have brightened roughly in step, with the BS being somewhat more prominent in November. This behavior is qualitatively consistent with an increase in the rate of mass supply from the secondary.

The UV flux level in our August/G160L data is below that seen in earlier *HST*/GHRS observations of UX UMa, and the system was somewhat fainter than usual even during those observations (Mason et al. 1995). Thus the brighter state the system was in during the November observations with the PRISM is probably more representative of the average mass transfer rate in UX UMa. Brightness changes of the magnitude we observed are not uncommon among NLs, many of which exhibit occasional high and low states (e.g., La Dous 1989b).

Based on the long-wavelength light curves of runs 3 and 4, we estimate that the half-width of the full disk eclipse is $\Delta\phi \simeq 0.1$. Using the geometric method of Sulkanen, Brasure, & Patterson (1981), this yields an estimate for the disk radius of $R_{\rm disk} \simeq 35 R_{\rm WD}$ when combined with Baptista et al.'s (1995) system parameters for UX UMa. No useful disk radius estimate can be made from the G160L light curves since the outer disk contributes so little to the total light at UV wavelength. We will analyze the eclipse geometry, including constraints on the disk radius, in more detail in Paper III. For the modeling of disk spectra carried out in the present study (§ 4), the estimate just quoted is sufficiently accurate.

3.2. *Eclipse Timings*

Figures 1 and 2 show that Baptista et al.'s (1995) ephemeris predicts the times of minima in 1994 August and November quite well. To quantify this agreement, we have measured accurate eclipse timings from the first-order white-light light curves in two ways. First, a parabolic function was fitted to the central part of the eclipse. This gives an estimate of the *time of minimum* in a given light curve.

Second, a numerical derivative was constructed from a slightly smoothed version of each light curve and inspected for extrema. The corresponding orbital phases should correspond to the ingress/egress phases of the WD and/or disk center, and their midpoint gives an estimate of *the mid-eclipse time* (time of conjunction). We estimate that the internal error on both types of $O-C$ measurements is less than 0.001 cycles. However, their reliability as estimates of times of conjunction could be subject to somewhat larger systematic uncertainties because the BS, the eclipse of which will not be centered on $\phi = 0$, also contributes to the total light from the system.

Our new eclipse timings for UX UMa are listed in Table 3. We find that (1) there are no obvious differences between the $O-C$ values derived for the August (runs 1 and 2) and November (runs 3 and 4) data sets with a given method, and (2) the $O-C$ values deduced from the parabolic fit to eclipse center, which have a mean of $+0.0033$ cycles, are systematically larger than those derived from the derivative light curve, which have a mean of $+0.0024$ cycles. The difference is probably due to the effect of the BS on the light curves. Since the BS eclipse is centered on some phase after conjunction, it will tend to skew measurements of eclipse timings toward later phases. This suggests that the $O-C$ values derived from the derivative light curve are more reliable estimates of times of conjunction, as expected.

We have not tried to refine Baptista et al.'s (1995) ephemeris on the basis of our new eclipse timings since the epochs of the new measurements add little to the long timeline of observations on which Baptista et al.'s ephemeris is based. The measured $O-C$ values are in any case quite small by UX UMa's standard (see Baptista et al. 1995, Fig. 5).

4. ANALYSIS OF SPECTRA

4.1. *Method*

In a first attempt to characterize and interpret the spectra of the system components that can be isolated in the data, we have fitted two types of (optically thick) models to the observations.

1. A single (effective) temperature, solar abundance stellar atmosphere (SA) model with the following parameters: temperature, gravity, normalization (projected area/distance^2).
2. A standard, steady state accretion disk radiating as an ensemble of solar abundance SAs with the following parameters: accretion rate, disk radius, normalization (distance).

The single-temperature SA model spectra were calculated by interpolation in temperature and gravity from a suitable grid of (angle-averaged) SA spectra that were generated from Kurucz (1991) ATLAS structure models using Hubeny's spectral synthesis code SYNSPEC (Hubeny, Lanz, & Jeffery 1994).

The disk models were constructed as area-weighted sums of SAs over the face of the accretion disk. In this summation, the standard relation for the run of effective temperature with radius in a steady state accretion disk was assumed (Pringle 1981), i.e.,

$$T_{\rm eff}(R) = T_*\left(\frac{R_{\rm WD}}{R}\right)^{3/4}\left[1-\left(\frac{R_{\rm WD}}{R}\right)^{1/2}\right]^{1/4}, \qquad (1)$$

where R is the distance from the WD on the disk and $R_{\rm WD}$ is the WD radius. T_* is a function of the mass accretion rate, $\dot{M}_{\rm acc}$, and the WD mass and radius:

$$T_* = \left(\frac{3GM_{\rm WD}\dot{M}_{\rm acc}}{8\sigma\pi R_{\rm WD}^3}\right)^{1/4}, \qquad (2)$$

with σ and G being the Stefan-Boltzmann and gravitational constants, respectively. For the local disk gravity, the approximate relation given by Herter et al. (1979) was adopted. In all disk models, we fixed the disk radius at $R_{\rm disk} = 35R_{\rm WD}$, as derived in § 3.1 from the PRISM light curves. Given the 3 month time delay between the first two and last two observing sequences, this estimate may not be appropriate for the G160L data. However, since the cool, outer disk contributes little to the total flux at UV wavelengths, disk model fits to tthe G160L spectra are insensitive to the adopted disk radius.

Considering the large wavelength range that is covered by the observations, we decided to account at least approximately for wavelength-dependent limb darkening in our disk models. To this end, we used SYNSPEC to calculate the specific intensities for an angle equal to UX UMa's inclination of $i = 71°$ from a suitable subset of the Kurucz ATLAS structure models and used these spectra, rather than ones corresponding to angle-averaged fluxes, in the construction of the disk model spectra. As shown by Diaz, Wade, & Hubeny (1996) for the UV wavelength region, where limb darkening is strongest, this should be a reasonable approximation for the optically thick disk models that are appropriate to UX UMa. To allow consideration of very high mass accretion rate models, in which the maximum effective temperature can exceed 50,000 K (the highest temperature for which Kurucz structure models exist), we also supplemented this grid of specific intensities with several spectra that were generated by SYNSPEC from TLUSTY (Hubeny 1988; Hubeny & Lanz 1995) structure models with 50,000 K $\leq T_{\rm eff} \leq$ 140,000, K.

Since the size of the emitting source is fixed in the disk models, the normalization constant required to match the observed flux measures the implied distance of the system. Distance estimates for UX UMa in the literature vary

TABLE 3

NEW ECLIPSE TIMINGS OF UX UMa[a]

Run	Cycle Number	HJD − 2,440,000[b]	$O-C$ (cycles)[b]	HJD − 2,440,000[c]	$O-C$ (cycles)[c]
1.....	28793	9,567.6353	+0.0025	9,567.6353	+0.0026
2.....	28794	9,567.8323	+0.0040	9,567.8319	+0.0021
3.....	29368	9,680.7215	+0.0034	9,680.7213	+0.0023
4.....	29371	9,681.3115	+0.0033	9,681.3113	+0.0025

[a] With respect to the ephemeris of Baptista et al. 1995.
[b] Measured from parabolic fit to eclipse center.
[c] Measured from derivative light curve.

between 216 and 345 pc (see Rutten et al. 1992 and Baptista et al. 1995 for overviews) with the most recent determination falling at the high end of this range (345 ± 34 pc; Baptista et al. 1995). Adopting the latter, formally most accurate estimate as the preferred distance toward the system, but allowing the uncertainty in this to be large enough to include all other previous distance determinations, we conservatively consider as viable all disk models for which the implied distance lies within the range 200–500 pc.

Neither of our two types of models is expected to reproduce the strong absorption and emission lines in UX UMa's UV spectrum, as these are most likely formed in the accretion disk wind from the system or in a transition region ("chromosphere") between the disk and the outflow (Drew 1993; Prinja & Rosen 1995; Knigge & Drew 1997; see also § 4.3). Consequently, wavelength regions containing strong lines were excluded in model fits to the G160L observations. All model spectra were smoothed to the appropriate instrumental resolution before comparing them to the data. In the following sections, we describe the results of these comparisons for runs 1 (G160L) and 3 (PRISM). Results for runs 2 (G160L) and 4 (PRISM) were essentially identical, as expected, since the observed spectra themselves are so similar (see Figs. 3 and 4).

4.2. *The Spectrum of the Accretion Disk*

The average pre-and post-eclipse spectra should be dominated by disk light. The posteclipse spectra, in particular, should represent the isolated spectrum of the accretion disk well since the BS contributes to the preeclipse flux, but is likely to be occulted at most or all posteclipse orbital phases (see § 3.1). We therefore use the posteclipse spectra as our best estimates of the spectrum of UX UMa's accretion disk in this section and fit them with both disk models and single-temperature SAs. The SA model fits are useful as a convenient parameterization of the observed spectral shape and as benchmarks against which the goodness of fit achieved by the physically more relevant disk models may be judged.

The best-fitting disk and SA models are shown along with the run 1 and 3 posteclipse spectra in Figure 5. While the accretion rates implied by the disk models, (1–2) × 10^{17} g s^{-1}, are not unreasonable a priori, the match to the data achieved by these models is not particularly good. Moreover, the distance implied by both "best" disk model fits is 200 pc, i.e., equal to the lower limit that we imposed in the least-squares minimization. Similar results were obtained in disk model fits to the mean preeclipse spectra and to the corresponding spectra in runs 2 and 4. However, the most disconcerting aspect of Figure 5 is that the disk models fit the data worse than single-temperature SAs. In fact, the best-fitting SA models, which have $T_{\rm eff} \simeq$ 12,500–14,500 K, provide a remarkably good match to the data at all observed wavelengths away from the Balmer jump, including the UV. (See Dickinson et al. 1997 for a similar finding for the NL CV V795 Her.) We have also tried to fit disk model spectra constructed as area-weighted sums of blackbodies to the pre- and posteclipse spectra, but these, too, fail to improve upon the fits achieved by single-temperature SA models.

According to Rutten et al. (1994), the spectral type of the secondary in the UX UMa lies in the range K7–M0. To illustrate how the observed spectra (and hence the model

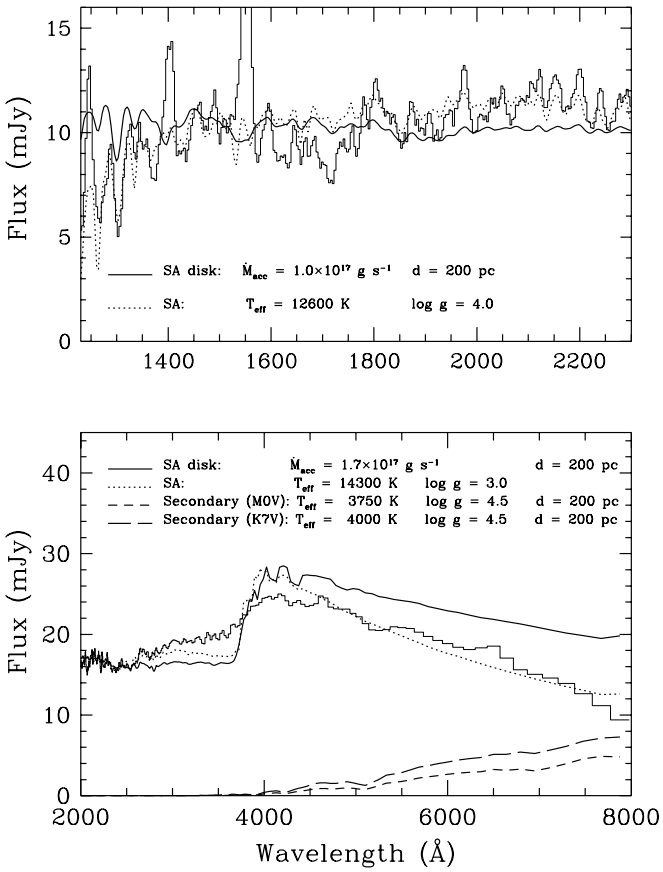

FIG. 5.—Model fits to the observed run 1 G160L (*top*) and run 3 PRISM (*bottom*) posteclipse spectra (shown as *histograms*). In both panels, the solid and dotted lines are the best-fitting disk model and single-temperature model stellar atmosphere spectra, respectively. For a distance toward UX UMa of 345 pc, the normalization of the stellar atmosphere models would require projected emitting areas, $A_{\rm proj}$, with a characteristic minimum linear size of $l_{\rm min} = (A_{\rm proj}/\pi)^{1/2} = 15R_{\rm WD}$ for the fit to the G160L data and $l_{\rm min} = 14R_{\rm WD}$ for that to the PRISM data. In the bottom panel, two model stellar atmospheres with spectral types likely to bracket that of the secondary star are also plotted (*short- and long-dashed lines*). These have been scaled according to the apparent secondary star radius (see text) and the 200 pc distance implied by the best-fitting disk model.

fits may be affected by the presence of this additional system component, we have included in Figure 5 SA model spectra for K7 and M0 main-sequence stars from the Buser & Kurucz (1992) compilation of ATLAS SA models (our grid of SYNSPEC-generated models does not extend to the required low effective temperatures). To allow a comparison with the disk model fit, the representative secondary star spectra in Figure 5 have been scaled to the flux expected from the secondary if the distance to the system were 200 pc. The scaled secondary star models in Figure 5 show that the contamination of the posteclipse spectra by light from the secondary is likely to be small, except perhaps at the longest optical wavelengths. There, the disk model spectrum already falls off more slowly with wavelength than the run 3 posteclipse spectrum, so that subtraction of the very red secondary star from the data prior to fitting the disk models is not likely to improve the fit.

Concerned that the apparent failure of the disk models may be caused by reddening or by some other flaw in our model-fitting procedure (perhaps related to the selection of continuum windows or to the highly nonuniform dispersion of the PRISM), we decided to compare these models against

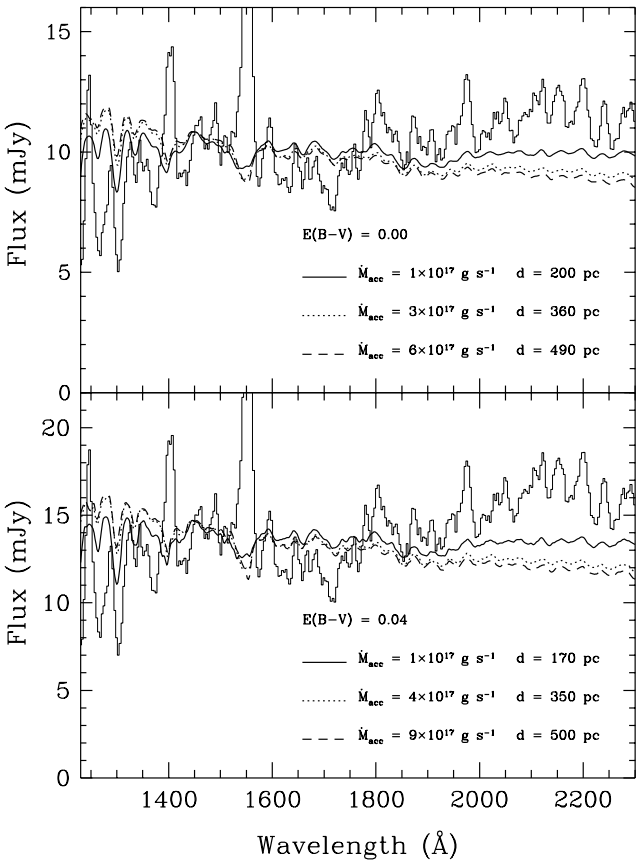

FIG. 6.—Comparison of the original (*top*) and maximally dereddened (*bottom*) run 1 G160L posteclipse spectra against disk models with varying accretion rates. All models have been normalized to the observed flux at 1450 Å. The accretion rates of the three models shown in each panel have been chosen so as to make the implied distances for this choice of normalization cover the allowed distance range of 200–500 pc.

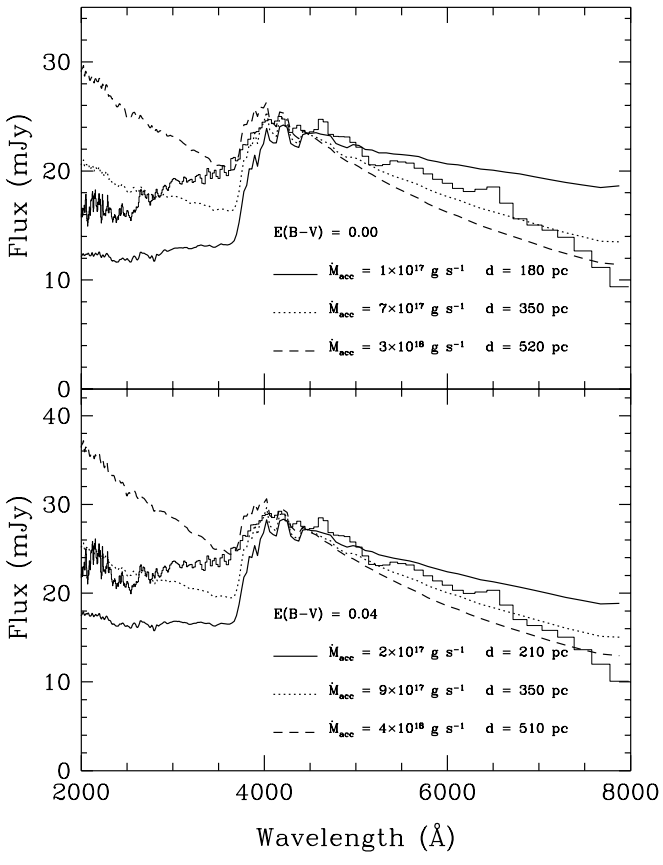

FIG. 7.—Comparison of the original (*top*) and maximally dereddened (*bottom*) run 3 PRISM posteclipse spectra against disk models with varying accretion rates. All models have been normalized to the observed flux at 4500 Å. The accretion rates of the three models shown in each panel have been chosen so as to make the implied distances for this choice of normalization completely cover the allowed distance range of 200–500 pc.

the data in another way. Thus, in each panel of Figures 6 and 7, three disk model spectra are plotted alongside the observations, with each model shown normalized to the data at a preselected continuum wavelength (1450 Å for the G160L data, 4500 Å for the PRISM data). The accretion rates corresponding to the models in each panel have been selected so as to make the implied distances for this choice of normalization completely cover the allowed range. Also, results are shown in Figures 6 and 7 for both minimal [$E(B-V) = 0.00$, *top panels*] and maximal [$E(B-V) = 0.04$, *bottom panels*] assumptions about the reddening toward UX UMa.

It is clear from Figures 6 and 7 that the mismatch between the data and the best-fitting disk models is real and cannot be attributed to the effects of reddening or explained as an artifact of the adopted fitting procedure. For example, even though a disk model with $\dot{M}_{\rm acc} = 9 \times 10^{17}$ g s^{-1} does produce an improved fit to the spectral shape of the maximally dereddened PRISM data, the Balmer jump in this model is still much too large. Furthermore, the match of all disk models to the dereddened G160L UV data is actually worse than that to the uncorrected spectrum. This is because the G160L data cover the broad 2175 Å dust absorption feature. Thus, while "dereddening" does produce spectra that are bluer than the original in most wavelength ranges, the effect is inverted at the longest UV wavelengths ($\gtrsim$1800 Å) which are affected by the 2175 Å feature. As a result, the discrepancy between the disk models and the data in that wavelength region is amplified, not reduced. It is also worth noting from Figure 6 that the UV slopes of disk model spectra are actually highly insensitive to the adopted accretion rate.

We may finally ask whether the poor fits to the data achieved by the disk models could be due to the contribution of the WD to the observed spectra. While it is possible that the WD does contribute nonnegligibly to UX UMa's UV flux (Baptista et al. 1995), it is unlikely that adding a corresponding component to the disk model spectra could improve the fit to the data in that wavelength region. This is because only a hot WD can contribute significantly at all, which means that any nonnegligibly WD spectral component must be very blue. This is unlikely to be of much help in our modeling since the disk models alone are already bluer than the observed UV spectra. This intuitively plausible prediction has been borne out quantitatively in previous analyses of UV CV spectra (Long et al. 1994; Knigge et al. 1997). Moreover, even a hot WD would not contribute much to the flux at optical wavelength, so the neglect of a WD component in our disk model fits to the PRISM data is almost certainly unimportant. From a broader perspective, it is of course nevertheless very important to try to isolate the WD component in our UV data. However, this is best achieved by means of careful, quantitative analyses of the eclipse light curves (see Baptista et al.

1995) rather than by examining the phase-averaged spectra. The results of such a light-curve analysis will be presented in Paper III.

Based on Figures 5–7 and the discussion up to now, we conclude that steady state SA disk models are unable to describe the data acceptably and, in fact, fare worse in this respect than simple, single-temperature model SAs. This conclusion appears to hold for all disk models with accretion rates that would retain consistency with existing distance estimates toward the system. This need not imply, of course, that the emitting region(s) in UX UMa are better described *physically* by a single-temperature SA than by a steady state accretion disk model. In fact, as noted in § 3.1, the wavelength dependence of the eclipse shape and depth does suggest a radially decreasint effective temperature distribution, as expected in the standard accretion disk picture. However, given that simple models based on steady state disk theory do not provide a good match to the spectral shape of real accretion disk systems, not even relative to single-temperature SAs, great care must be taken in attempts to infer disk parameters on the basis of any such models.

As an aside, we note that this caution is as relevant to eclipse mapping studies, including those based on image reconstruction techniques, as it is to studies relying directly on model fits to observed accretion disk spectra. The reason for this is that the accretion rate cannot be inferred directly from a disk's surface brightness distribution; what is needed instead is the radial run of (effective) temperatures across the disk. It is this intermediate step, the transformation of surface brightness into temperature, which requires the specification of an emissivity law (as well as a distance estimate). In practice, BB emissivities are usually assumed at this stage. Thus,, even though disk images obtained with the maximum entropy method, for example, are independent of any assumptions about the spectral properties of the disk, the radial temperature distributions and accretion rates derived from such images are not. It should also be kept in mind that both the shape and normalization of radial temperature distributions derived in this way are sensitive to errors in the adopted distance estimates.

Returning to the disk model fits, we note that the two main failings of the models are (1) their excessively blue color at UV wavelengths, and (2) the magnitude of the predicted Balmer jump, which is much larger than observed.

Both of these problems have long histories. Wade (1988) first noted that SA disk model spectra were systematically bluer than the spectra of NL CVs observed with the *International Ultraviolet Explorer* (*IUE*). He found that the problem could only be alleviated if uncomfortably low accretion rates were adopted, which in turn produced a large UV flux deficit in the model spectra for the accepted distances toward the systems in his sample. The same problem has since been encountered in analyses of Hopkins Ultraviolet Telescope (HUT) observations of high-state, nonmagnetic CVs (Long et al. 1991, 1994; Knigge et al. 1997). Thanks to HUT's coverage of wavelengths all the way down to the Lyman limit, the latter studies were able to show more conclusively that models with low accretion rates do not offer a viable solution, since they fail to fit the observed spectra shortward of their turnover at about 1000 Å. Similarly, the discrepancy between observed and predicted Balmer jumps is also not new. Wade (1984) and La Dous (1989a), for example, have also constructed SA disk model spectra covering the optical and UV ranges. Their models, as ours, were found to produce much larger Balmer jumps than are observed. We will discuss possible resolutions to these problems in § 5.

4.3. *The Spectrum of the Uneclipsed Light*

UX UMa's eclipses are not total: some residual flux emerges at all UV and optical wavelengths even at mideclipse (see Figs. 1 and 2). Some of this uneclipsed light is due to the secondary star, but the outer parts of the disk on the far side from the secondary also contribute since UX UMa's accretion disk is never fully occulted. In addition to these two components, there may also be other sources of radiation that remain uneclipsed by virtue of their vertical extent. For example, (some of) the spectral lines in the UV region are almost certainly formed in UX UMa's accretion disk wind (Knigge & Drew 1997), and part of the BS (see § 4.4) may also have the required geometrical and emissive properties to contribute to the uneclipsed light (the required vertical extent would be $z_{BS} \gtrsim 18R_{WD}$).

The mean mideclipse spectra derived from runs 1 and 3 are shown along with the best-fitting single-temperature SA model spectra in Figure 8. The G160L UV spectrum has a

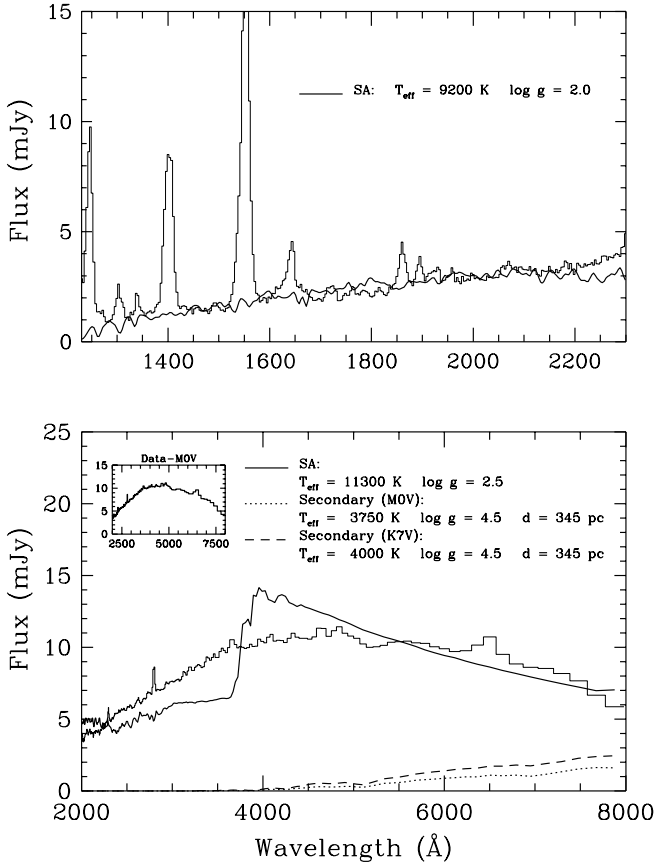

FIG. 8.—Model fits to run 1 G160L (*top*) and run 3 PRISM (*bottom*) mideclipse spectra (*histograms*). In each panel, the solid line corresponds to the best-fitting single-temperature model stellar atmosphere. For a distance toward UX UMa of 345 pc, the normalization of the models requires projected emitting areas with minimum linear sizes of $l_{min} = 20R_{WD}$ (G160L) and $l_{min} = 12R_{WD}$ (PRISM). In the bottom panel, two model stellar atmospheres with spectral types likely to bracket that of the secondary star are also plotted (*dotted and dashed lines*). These have been scaled according to the apparent secondary star radius (see text) and a distance of 345 pc. The inset in the bottom panel shows the result of subtracting the M0 V main-sequence star spectrum from the data.

relatively flat continuum and is dominated by emission lines. It is easy to show that the secondary star contributes negligibly to the uneclipsed light in this wave band for any plausible combination of distance and spectral type. The UV continuum shape is nevertheless reasonably well described by a single-temperature SA with $\log g = 2.0$ and $T_{\rm eff} = 9200$ K. If we take these parameters to be meaningful, they must be representative of the physical conditions in the outer accretion disk. However, for a distance toward the system of 345 pc, the normalization of the SA model fit predicts that the emitting source has a projected area, $A_{\rm proj}$, the minimum linear size orf which is $l_{\rm min} = (A_{\rm proj}/\pi)^{1/2} = 20R_{\rm WD}$. If we identify this source with the uneclipsed part of the accretion disk, this size estimate must be increased by a factor of $(\cos i)^{-1/2} = 1.75$ to $l_{\rm min} = 35R_{\rm WD}$ due to foreshortening. This is equal to the disk radius estimate derived from the PRISM data and therefore too large to describe the fraction of the disk that remains unocculted at mideclipse. Thus the identification of the uneclipsed UV light with just the outer parts of an optically thick, geometrically thin disk is probably not viable, unless the distance toward UX UMa is significantly less than 345 pc. Of course, the outer disk may be neither optically thick nor geometrically thin, and the accretion disk wind and/or parts of the BS region may also contribute to the mideclipse UV continuum flux.

The classical CV wind lines, N v 1240 Å, Si iv 1400 Å, and C iv 1550 Å, are hardly occulted (see Fig. 3), as expected if they are formed in the vertically extended outflow. It should be noted, however, that recent *HST*/GHRs eclipse observations of the C iv line in UX UMa show that the weak line eclipses are at least partly due to narrow *absorption* features in the out-of-eclipse line profiles, which *are* occulted during eclipses (Mason et al. 1995). Knigge & Drew (1997) modeled these data and showed that the region contributing net absorption to the line profiles can be plausibly identified with a relatively dense, slow-moving transition region between the accretion disk and the fast wind (see also Baptista et al. 1995 and § 5).

Knigge et al. (1997) used the same model to fit five strong UV resonance lines in a HUT spectrum of the DN Z Cam in outburst and showed that several other lines that are typically seen in the UV spectra of high-state CVs might be produced in the dense transition region predicted by this wind model. This idea is supported by our data, inasmuch as not just the classical wind features but just about all identifiable spectral lines—some of which appear in absorption away from eclipse (e.g., Si iii 1265 Å, C ii 1335 Å, N iv 1718 Å)—become clear emission features in the mideclipse G160L spectra.

Whether a spectral line that is formed in such a region will appear as an absorption or an emission feature depends on how much of the line-forming region is seen projected against the bright accretion disk at the relevant inclination and orbital phase. In an eclipsing system, such as UX UMa, much of the disk is occulted at mideclipse. Consequently, the only parts of the line-forming region that are visible at that phase are those that do not lie "in front of" the disk as seen from Earth. Inevitably, therefore, an emission-line spectrum will be observed in that case at orbital phase $\phi = 0.0$. If thermal line emission from (as opposed to scattering in) such a transition region is sufficiently strong, the spectral features formed within it may also appear in emission even when the disk does lie within our line of sight.

The run 3 PRISM mideclipse spectrum in Figure 8 is also much redder than its out-of-eclipse counterpart. However, its continuum shape is not well described by a single-temperature SA (the best-fitting model has $\log g = 2.5$ and $T_{\rm eff} = 11{,}300$ K). The main problem is that for the relatively low temperature needed to fit the overall shape of the spectrum, SA models predict the presence of an extremely strong Balmer jump. On the other hand, a Balmer absorption edge is not visible in the data (the jump may even be slightly in emission).

The temperature of the best-fitting SA model is still much higher than expected for the secondary star. To estimate the likely contribution of the secondary to the optical spectrum of the uneclipsed light, two representative spectra are again shown in Figure 8. The stellar radius and spectral types adopted for these secondary star model spectra are the same as for those in Figure 5, but the predicted fluxes have been rescaled to correspond to our preferred distance estimate of 345 pc. For these parameters, the secondary contributes measurably to the uneclipsed light above 4000 Å but does not dominate even at the longest wavelengths. The shape of the observed mideclipse spectrum also makes it clear that the secondary cannot be the sole (and is probably not even the main) contributor to the uneclipsed optical light. Instead, the absence of a Balmer jump in the spectrum suggests that optically thin material may contribute to the mideclipse spectrum, once again implicating the outer disk, the BS, and/or the accretion disk wind.

4.4. *The Spectrum of the Bright Spot*

If the light-curve asymmetries in Figures 1 and 2 are due to the BS, its spectrum can be isolated approximately by taking the difference between the average pre- and posteclipse spectra. These difference spectra are shown in Figure 9 for runs 1 and 3, along with the best-fitting single-temperature SA models.

The continuum shape of the UV BS spectrum is fairly similar to that of the accretion disk (cf. Fig. 5) and thus has a comparable color temperature (about 16,000 K). The minimum linear size [calculated once again as $l_{\rm min} = (A_{\rm proj}/\pi)^{1/2}$] provided by the SA model fit to the G160L data is about $5R_{\rm WD}$ for an assumed distance of 345 pc. This is probably a reasonable estimate for the size of the BS. We nevertheless caution that both temperature and size estimates may be unreliable for reasons that will become clear below.

All of the spectral lines that can be identified in the UV BS spectrum appear to be in absorption (Si iii 1300 Å, Si iv 1400 Å, C iv 1550 Å, and Al iii 1860 Å). This is interesting, since at least two of the same features (Si iv 1400 Å and C iv 1550 Å) are in emission in the pre- and posteclipse spectra. Given that most of the UV lines are probably formed in some part of the UX UMa's accretion disk wind, one possibility is that some of the radiation emitted by the BS is scattered out of our line of sight by the outflow. In this picture, the line of sight to the BS must pass through the wind. Alternatively, the spot may be optically thick and produce an absorption-line spectrum similar to a SA. Finally, the spot may be (partially) optically thin in the continuum, and act as a veiling curtain for the radiation emitted by the disk and/or the wind. In this case, our line of sight to the disk and/or wind must pass through at least part of the BS at preeclipse phases, which requires the spot to have a significant vertical extent.

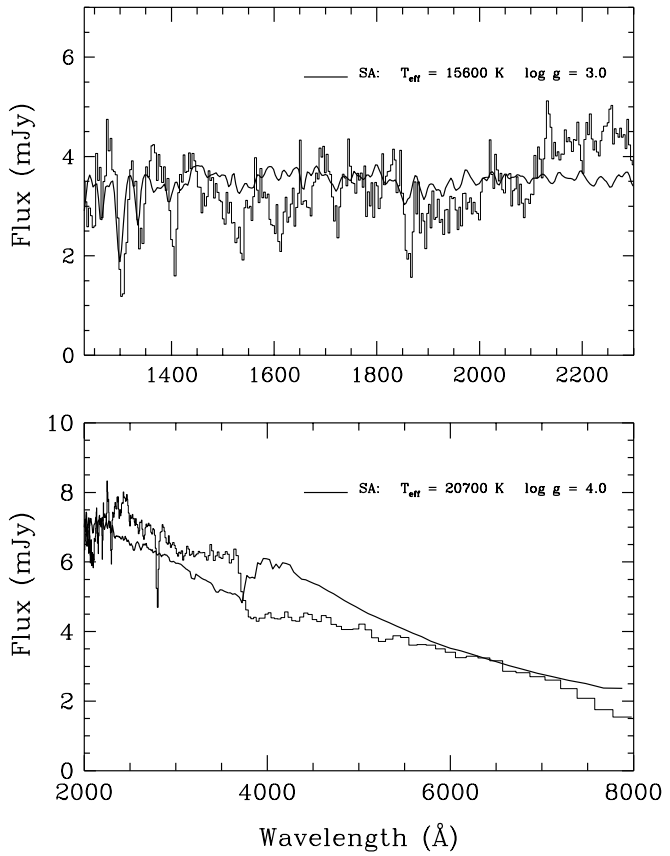

FIG. 9.—Model fits to the bright spot spectra constructed from the run 1 G160L data (*top*) and the run 3 PRISM data (*bottom*). Bright spot spectra have been calculated for each observing sequence by subtracting the average posteclipse spectrum from the average preeclipse spectrum. In each panel, the data are plotted as a histogram and the solid line corresponds to the best-fitting single-temperature model stellar atmosphere. For a distance toward UX UMa of 345 pc, the normalization of the models would require projected emitting areas with minimum linear sizes of $l_{min} = 5R_{WD}$ in both cases.

The PRISM BS spectrum is even more striking. It, too, exhibits line absorption features at near-UV wavelengths, but more importantly, the Balmer jump is in emission. This suggests that the BS is at least partially optically thin and strengthens the case for the veiling interpretation of the spot's UV absorption-line spectrum. It does not confirm it beyond doubt for the G160L data, at least, because of the significant change in brightness (accretion rate) that took place between August and November and which might have altered the structure of the BS. In any case, given the signature of optically thin material in the PRISM BS spectrum, the estimates of the BS size and temperature provided by the best-fitting SA model to these data sets, $l_{min} \simeq 5R_{WD}$ and $T_{BS} \sim 2 \times 10^4$ K, must be regarded with caution. This warning may also apply to the estimates derived for the G160L data, if the BS region was in fact also partially optically thin in August.

We close this section by acknowledging that we cannot rule out that the light-curve asymmetries in our data are due to absorption at posteclipse orbital phases, rather than to the contribution of the BS to the light at preeclipse phases. This possibility finds some support in the fact that there are instances among existing eclipse observations of UX UMa (as well as among those of other nonmagnetic CVs) in which the ratio of pre- and posteclipse flux levels is less than 1 (see Mason, Drew, & Knigge 1997 and references therein). If the light-curve asymmetries in our data are in fact due to absorption, the difference spectra on which we have relied in this section are not physically meaningful. However, in this case the ratio of posteclipse to preeclipse fluxes could be used to constrain the physical condition in the absorbing material. This idea will be explored in more detail in Paper IV.

5. DISCUSSION

As noted in § 4.2, SA disk models, which should offer the closest representation of a real accretion disk spectrum among the models we have tried, do poorly in matching the observed spectra of UX UMa and other high-state CVs. More importantly, the UV colors predicted by SA disk models are too blue and the magnitude of the Balmer jump is too large.

There are at least three possible reasons for these discrepancies. First, the poor fits to the data may simply be due to the inadequacy of our disk models. Certainly, given the very different geometries involved, the atmospheres of real accretion disks may differ considerably from those of ordinary stars. Some headway has already been made in the construction of more self-consistent disk models, but the results so far are still inconclusive. For example, Shaviv & Wehrse (1991) simultaneously solved the (vertical) disk structure and radiative transfer equations and presented the resulting self-consistent accretion disk model spectra. These authors appeared to conclude that their models are able to resolve the discrepancies between theory and observations. Long et al. (1994), on the other hand, showed that similarly self-consistent disk model spectra constructed on the basis of disk model atmospheres calculated with Hubeny's code TLUSDISK (Hubeny 1988, 1991) differed little from those predicted by disk models constructed as sums of ordinary SAs in the UV waveband. Correspondingly, Long et al. (1994) concluded that current state-of-the-art disk models could not resolve the UV color problem. The difference between these conclusions may simply be due to the different wavelength ranges that were used in the comparisons with observations, as well as perhaps to different views about what constitutes success in the comparison of models and data. However, the somewhat different assumptions concerning viscosity and energy release in the vertical direction that are adopted in TLUSDISK and in the disk model calculations of Shaviv & Wehrse (1991) may also play a role. We finally note in this context that some potentially important aspects of the disk physics, such as the radiative transport in the radial direction and the irradiation of the disk by the WD and perhaps the boundary layer (BL), remain to be explored.

A second way to account for the failure of SA disk models is to question the assumptions made in the standard steady state disk model itself. For example, Long et al. (1994) showed that the UV colors of SA disk models could be reconciled with the observations if the hot, inner parts of the disk (out to a few R_{WD}) were removed. Physically, both the truncation of the disk by the magnetic field of the WD, a situation analogous to that in intermediate polars, or the removal of accretion energy by a powerful disk wind might produce the observational signature of a "missing" (or cooler than expected) inner disk. The former possibility has some additional appeal in that it might explain the short-period oscillations that have been observed in UX UMa

and other nonmagnetic CVs (see Paper II). However, one problem with this idea is that any type of effective disk truncation may help to account for the observed UV colors, but would probably worsen the Balmer jump discrepancy (cf. the spectra of disk annuli as a function of radius in La Dous 1989a and Shaviv & Wehrse 1991).

A third possibility is that there are additional sources of radiation in the system that must be included in model fits to the observed spectrum. However, as noted in § 4.2, any additional optically thick components, e.g., due to the WD or BL, are unlikely to resolve the UV color problem or to contribute significantly at optical wavelengths. Thus, the only remaining option is to identify the presumed additional emitting source with an optically thin plasma (Hassall 1985).

The idea that optically thin emission may contribute to the observed spectrum in UX UMa finds some empirical support in the fact that the Balmer jump is strongly in emission in the PRISM spectra of the BS and is either absent or perhaps very weakly in emission in the PRISM mideclipse spectra. Independent "theoretical" support comes from recent efforts to model the shapes, strengths, and eclipse behavior of the C IV 1550 Å resonance lines in the UV spectra of two high-inclination NL CVs (Shlosman, Vitello, & Mauche 1996; Knigge & Drew 1997). Both of these studies assumed that line formation occurs in a rotating, biconical accretion disk wind and derived the required geometric and kinematic outflow parameters from fits to the observed line characteristics. Knigge & Drew (1997), in particular, modeled high-quality *HST*/GHRS eclipse observations of UX UMa itself. A fundamental property of their preferred wind model is very slow outflow acceleration close to the disk plane, giving rise to an almost static, relatively dense ($n_e \simeq 4 \times 10^{12}$ cm^{-3}) and vertically extended ($H \sim 10R_{\rm WD}$) "transition region" between the disk surface and the fast-moving parts of the wind. Such a region, which we shall call an accretion disk chromosphere (ADC) hereafter, without meaning to imply any direct correspondence with stellar chromospheres, could, in principle, produce significant amounts of optically thin recombination radiation.

To gain some insight into how much optically thin emission is required to make a significant difference to the observed spectra, we have followed Hassall (1985) in determining the emission measure (EMs) required to fill in the Balmer jump absorption in the disk model spectra with Balmer jump emission produced by H I recombination radiation. However, unlike Hassall (1985), we have calculated the required EM for a variety of plasma temperatures and accretion rates, and also determined for each combination of disk model and H I plasma the implied distance if this combination is to match the flux of the observed run 3 posteclipse spectrum at 4500 Å.

The results of this exercise are shown in Figure 10. It is easy to see from this that for accretion rates $\dot{M}_{\rm acc} \gtrsim 1 \times 10^{17}$ g s^{-1} and distances in the range 200 pc $< d <$ 500 pc, emission measures in the range 10^{56} cm$^{-3} \lesssim$ EM $\lesssim 10^{58}$ cm^{-3} and temperatures $T \lesssim 4 \times 10^5$ K are required. How reasonable is this? Assuming a uniform, fully ionized ADC with the parameters derived by Knigge & Drew (1997), we find EM $\simeq n_e^2 \times \pi R_{\rm disk}^2 \times H = 5.7 \times 10^{56}$ cm^{-3}. Regarding the temperature of the ADC, Knigge & Drew's (1997) found that $T \simeq 30{,}000$ K produced the required amount of thermal C IV emission in their "best-bet" wind model. (It should be noted, however, that the C IV ionization fraction in their wind model was not calculated but simply set to a plausible average value; also, collisional effects were treated only approximately.)

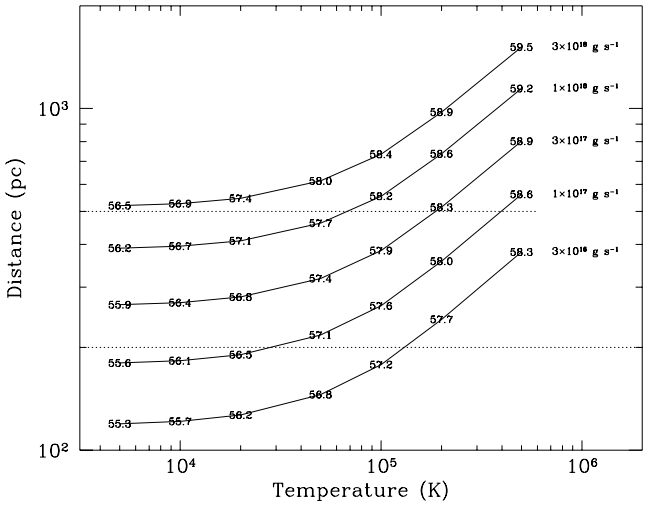

FIG. 10.—Emission measures required to fill in the Balmer jump in disk model spectra. Each connected sequence of numbers in this figure gives the emission measures needed to completely fill in the Balmer jump in the spectrum of a disk model with given accretion rate by adding an optically thin H I recombination continuum component. The emission measures are placed on the plot according to the electron temperature of the optically thin component (*x*-axis) and the implied distance (*y*-axis) if the combined disk + recombination model is to match the run 3 posteclipse spectrum at 4500 Å. The horizontal dotted lines mark the upper and lower limits of 200 and 500 pc, respectively, on the distance toward UX UMa.

The idea that optically thin ADC emission is contributing to the observed spectra, and may be (partly) responsible for the poor fits achieved by SA disk models, can be tested more directly by comparing combined disk + ADC model spectra to the observations. To this end we have used CLOUDY v90.03 (Ferland 1996) to calculate the emission expected from a solar abundance coronal (i.e., collisionally ionized) plasma at a variety of temperatures. For definiteness, $n_{\rm H} = 5 \times 10^{12}$ cm^{-3} was assumed in all of these models. Figure 11 shows the resulting optically thin model spectra.

Collisonal equilibrium is probably not a very good approximation to the conditions in the ADC, since photoionization by disk and perhaps WD or BL photons is probably the dominant ionization process. However, a photoionization model of the ADC would have to account in some way for the two-dimensional character of the ADC geometry and its illumination. This introduces complications that are unwarranted for our present, purely exploratory calculations, which are only intended to illustrate qualitatively the effect of an optically thin ADC on the shape of the emergent continuum. We note for reference that in the coronal models hydrogen (helium) is essentially fully ionized for $T \gtrsim 2 \times 10^4$ K ($T \gtrsim 8 \times 10^4$ K). In a photoionized ADC, these and all other elements will be more strongly ionized at relatively lower temperatures. Correspondingly, the spectral lines and line ratios predicted by our collisional equilibrium ADC models will certainly not be representative of photoionized ADCs at similar temperatures. In our comparisons of disk + ADC models to the data below, we therefore consider only the continuum contribution of the ADC and exclude the lines produced by the optically thin plasma.

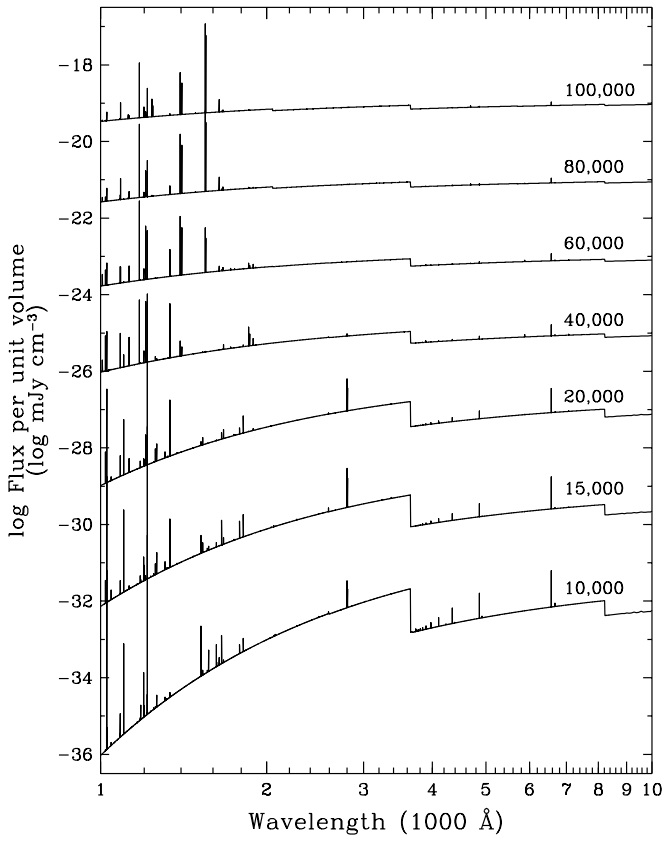

FIG. 11.—Spectra emitted by 1 cm^{-3} of solar abundance plasmas in coronal (collisional) equilibrium are shown for a variety of electron temperatures. The lowest temperature spectrum is shown on the true scale; all others have been displaced vertically by successive factors of 100. Note that the line-to-continuum contrast in these spectra corresponds to an intrinsic line width equal to the speed of light. (This convention is the default in CLOUDY c90.03.) Thus, for a more realistic line width of 3000 km s^{-1}, for example, the observed contrast would be 100 times larger.

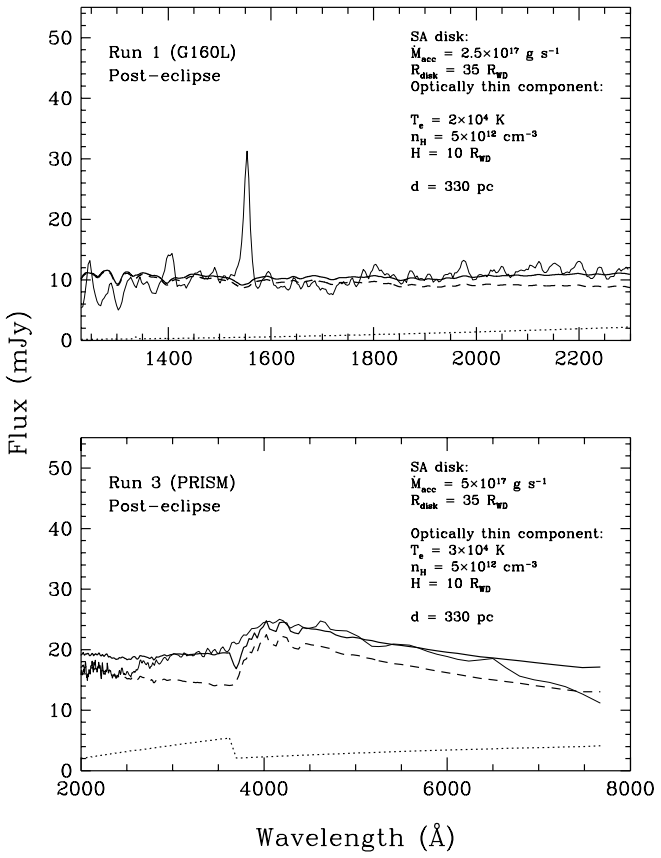

FIG. 12.—Illustrative fits to the run 1 (*top*) *and run* 3 (*bottom*) posteclipse spectra, shown as thin solid lines. The models (*thick solid lines*) are combinations of optically thin recombination continua (*dotted lines*) and SA disk models (*dashed lines*). The parameters adopted for the fits are noted in the figures; the volume of the optically thin gas is $V = \pi R_{\rm disk}^2 H$, so if the optically thin material is located in a roughly cylindrical region above the surface of the accretion disk, H is the corresponding vertical scale height.

Given our very simplified treatment of the ADC emission, including also the neglect of all radiative transfer effects (such as [self-] absorption), we have not carried out any detailed least-squares fits of disk + ADC models to the observed spectra. Instead, we illustrate the type of match to the data that can be achieved by adding an optically thin ADC continuum component to the disk models by means of just one example, shown in Figure 12. This shows that, in principle, the addition of an optically thin ADC continuum to an optically thick disk model spectrum may well resolve both the UV color problem and the Balmer jump discrepancy for reasonable disk and ADC parameters. More specifically, the model in Figure 12 employs a disk radius that is consistent with the total eclipse width (§ 3.1), reasonable disk accretion rates that correlate with the brightness change between August and November, ADC parameters that are very similar to those derived by Knigge & Drew (1997), and a distance to the system close to the most recent estimate of Baptista et al. (1995). Since only a fraction of the ADC will be occulted by the secondary star, it will also provide an additional source of uneclipsed, optically thin radiation that may help to account for the relatively high mideclipse flux levels and for the absence of the Balmer jump in the optical mideclipse spectra. How much of the ADC light should be expected to remain uneclipsed will depend on the detailed geometry of and the run of physical conditions within this region.

We stress that our disk + ADC models are only illustrative (since our treatment of the ADC is so approximate) and that there are a number of questions that will have to be answered by modeling the combination of disk, wind, and transition region in a more self-consistent manner. For example, regardless of the wind driving mechanism, one might expect the wind mass-loss rate (and hence the density in the ADC) to scale approximately with the accretion rate through the disk (e.g., Livio 1996). Correspondingly, we would have preferred to scale the emission measures used in the disk + ADC models for the G160L and PRISM data by the square of the ratio of the assumed accretion rates in these fits. (In our constant-density models, the appropriate adjustment would have been to the ADC scale height, H.) However, we found that matching the UV color in the G160L data always required an emission measure similar to, or even greater than, that required to smooth out the Balmer jump in disk + ADC model fits to the PRISM data. We also note again that we have not included the spectral lines produced by ADC models in the comparison with the data, since these are likely to be worst affected by the assumption of coronal equilibrium. It nevertheless seems likely that any optically thin ADC will produce strong line

emission of some kind. It remains to be seen if such line emission can be consistent with observations.

6. CONCLUSIONS

We have presented and analyzed *HST*/FOS eclipse observations of the NL CV UX UMa. Two eclipses each were observed with the G160L grating in 1994 August and the PRISM in November of the same year. The main results of our analysis are as follows:

1. The system was approximately 50% brighter in November than in August. If interpreted as resulting from a change in accretion rate, this indicates an increase in $\dot{M}_{\rm acc}$ by $\gtrsim 50\%$ between the observations.

2. From short to long wavelengths, UX UMa's eclipses become broader and shallower, and the (out-of-eclipse) flux level drops. These characteristics are consistent with the gradual occultation of an accretion disk with a radially decreasing temperature distribution.

3. The light curves exhibit significant asymmetries about orbital phase $\phi = 0.0$ that are likely due to the BS at the disk edge. The UV spectrum of the BS, constructed as the preeclipse minus posteclipse difference spectrum, exhibits absorption lines, suggesting that part of the BS may be optically thin in the continuum and veil the inner disk and/or the outflow from UX UMa in these lines. More direct evidence for the presence of optically thin material in the BS region is provided by the fact that the Balmer jump is strongly in emission in the optical BS spectrum derived from the PRISM observations.

4. Disk models constructed as ensembles of SAs provide poor descriptions of the observed accretion disk spectra if the latter are identified with the spectra observed at orbital phases away from the eclipse. Compared to the data, disk model spectra are too blue at UV wavelengths and exhibit excessively strong Balmer jumps in the optical region. Surprisingly, suitably scaled, single-temperature model SAs with $T_{\rm eff} \simeq 12{,}500$–$14{,}500$ K provide a significantly better match to both the UV and optical data. Based on this, we conclude that great care must be taken in attempts to derive accretion rates from direct comparisons of disk models to observations. This caution is relevant even to eclipse mapping studies, since the transformation of surface brightness to disk temperature *always* requires the specification of an emissivity law. If the mismatch between disk models and CV spectra is due to "contamination" of the uneclipsed light by additional, nondisk radiation (see item 5 below), the problems just mentioned might be overcome by accounting explicitly for the additional spectral component(s) when analyzing the data.

5. One way to reconcile simple SA disk models with the observed spectra is to postulate the presence of a significant amount of optically thin gas in the system. The corresponding additional spectral component would both flatten the UV spectral slope and fill in the Balmer jump of the optically thick disk spectrum. The required optically thin material could be located in a transition region between the disk photosphere and the fast wind from the system. The existence of such an "accretion disk chromosphere" was proposed by Knigge & Drew (1997) based on detailed modeling of *HST* eclipse observations of the C IV wind line in UX UMa. A simple SA disk + ADC model that uses ADC parameters similar to those suggested by Knigge & Drew (1997) does produce an improved, although still far from perfect, fit to the observed UV and optical disk spectra. However, a self-consistent calculation, in which photoionization and radiative transfer effects are accounted for, will be needed to properly test this idea. At least until then, other ways to resolve the discrepancy between SA disk models and observed spectra (e.g., magnetic disk truncation, better disk models) also remain viable.

6. The presence of a multitude of uneclipsed emission lines in the UV mideclipse spectra (some of which appear as absorption features at out-of-eclipse phases) supports the suggestion made by Knigge et al. (1997) that many, if not most, of the spectral lines in the UV spectra of high-state nonmagnetic CVs might arise in the kind of ADC/wind region envisioned by Knigge & Drew (1997).

We gratefully acknowledge the support of NASA through *HST* grant GO-5448, without which this work would not have been possible. In addition, R. A. W. acknowledges financial support from NASA through grants NAGW-3171 and from STScI through grant GO-3683.03-91A, both to the Pennsylvania State University. We would also like to thank Chris Mauche for his contribution to this project and for a number of useful discussions related to this paper. We are also grateful to the referee for a very helpful report.

REFERENCES

Baptista, R., Horne, K., Hilditch, R. W., Mason, K. O., & Drew, J. E. 1995, ApJ, 448, 395
Baptista, R., et al. 1998, ApJ, submitted (Paper IV)
Buser, R., & Kurucz, R. L. 1992, A&A, 264, 557
Diaz, M., Wade, R. A., & Hubeny, I. 1996, ApJ, 459, 236
Dickinson, R. J., Prinja, R. K., Rosen, S. R., King, A. R., Hellier, C., & Horne, K. 1997, MNRAS, 286, 447
Drew, J. E. 1993, in Proc. Second Technicon Haifa Conference on Cataclysmic Variables and Related Physics, ed. O. Regev (Ann. Israoti Phys. Soc.) (Bristol: IOP), 128
Eracleous, M., & Horne, K. 1994, ApJ, 433, 313
Ferland, G. J. 1996, Univ. Kentucky Internal Rep.
Hassall, B. J. M. 1985, MNRAS, 216, 335
Herter, T., Lacasse, M. G., Wesemael, F., & Winget, D. E. 1979, ApJS, 39, 513
Horne, K. 1985, MNRAS, 213, 129
Horne, K., & Eracleous, M. 1993, FOS instrument Sci. Rep. CAL/FOS-091 (Baltimore: STScI)
Hubeny, I. 1988, Comput. Phys. Commun., 52, 103
———. in IAU Colloq. 129, Structure and Emission Properties of Accretion Disks, ed. C. Bertout, S. Collin-Souffrin, J. P. Lasota, & J. Thran Thran Van (Gif-sur-Yvette: Editions Frontières), 227
Hubeny, I., & Lanz, T. 1995, ApJ, 439, 875
Hubeny, I., Lanz, T., & Jeffery, C. S. 1994, Newsletter on Analysis of Astronomical Spectra (St. Andrews: St. Andrews Univ.), 20, 30
Knigge, C., & Drew, J. E. 1997, ApJ, 486, 445
Knigge, C., Long, K. S., Blair, W. P., & Wade, R. A. 1997, ApJ, 476, 291
Knigge, C., Drake, N., Long, K. S., Wade, R. A., Horne, K., & Baptista, R. 1998a, ApJ, 499, in press (Paper II)
Knigge, C., et al. 1998b, in preparation (Paper III)
Kukarkin, B. V. 1977, MNRAS, 180, 5P
Kurucz, R. L. 1991, in Stellar Atmospheres: Beyond Classical Models, ed. L. Crivellari, I. Hubeny, & D. G. Hummer (Dordrecht: Kluwer), 441
La Dous, C. 1989a, A&A, 211, 131
———. 1989b, in Cataclysmic Variables and Related Objects, ed. M. Hack & C. La Dous (NASA/CNRS Monogr. Ser. on Non-thermal Phenomena in Stellar Atmospheres; Greenbelt: NASA), 15
Livio, M. 1996, in ASP Conf. Ser. 121 (IAU Colloq. 163), Accretion Phenomena and Related Outflows, ed. D. T. Wickramasinghe, G. V. Bicknell, & L. Ferrario (San Francisco: ASP), 8
Long, K. S., et al. 1991, ApJ, 381, L25
Long, K. S., Wade, R. A., Blair, W. P., Davidsen, A. F., & Hubeny, I. 1994, ApJ, 426, 704
Mason, K. O., Drew, J. E., Córdova, F. A., Horne, K., Hilditch, R., Knigge, C., Lanz, T., & Meylan, T. 1995, MNRAS, 274, 271
Mason, K. O., Drew, J. E., & Knigge, C. 1997, MNRAS, 209, L23

Meyer, F., & Meyer-Hofmeister, E. 1983, A&&, 121, 29
Nather, R. E., & Robinson, E. L. 1974, ApJ, 190, 637
Pringle, J. E. 1981, ARA&A, 19, 137
Prinja, R. K., & Rosen, S. R. 1995, MNRAS, 273, 461
Rutten, R. G. M., Dhillon, V. S., Horne, K., & Kuulkers, E. 1994, A&A, 283, 441
Rutten, R. G. M., van Paradijs, J., & Tinbergen, J. 1992, A&A, 260, 213
Shaviv, G., & Wehrse, R. 1991, A&A, 251, 117
Shlosman, I., Vitello, P. A. J., & Mauche, C. W. 1996, ApJ, 461, 377
Smak, J. 1983, Acta Astron., 272, 234
Sulkanen, M. E., Brasure, L. W., & Patterson, J. 1981, ApJ, 224, 579
Verbunt, F. 1987, A&AS, 71, 339
Wade, R. A. 1984, MNRAS, 208, 381
———. 1988, ApJ, 335, 394
Warner, B., & Nather, R. E. 1972, MNRAS, 159, 429